S. Saffar
Department of Structural Engineering,
Norwegian University of
Science and Technology,
NO-7491 Trondheim, Norway

S. Gouttebroze
SINTEF Materials and Chemistry,
NO-0315 Oslo, Norway

Z. L. Zhang[1]
Department of Structural Engineering,
Norwegian University of
Science and Technology,
NO-7491 Trondheim, Norway
e-mail: zhiliang.zhang@ntnu.no

The Effect of Microstructure, Thickness Variation, and Crack on the Natural Frequency of Solar Silicon Wafers

Vibration is one of the most common loading modes during handling and transport of solar silicon wafers and has a great influence on the breakage rate. In order to control the breakage rate during handling and facilitate the optimization of the processing steps, it is important to understand the factors which influence the natural frequency of thin silicon wafers. In this study, we applied nonlinear finite element method to investigate the correlation of natural frequency of thin solar silicon wafer with material microstructures (grain size and grain orientation), thickness variation and crack geometry (position and size). It has been found that the natural frequency for anisotropic single crystal silicon wafer is a strong function of material orientation. Less than 10% thickness variation will have a negligible effect on natural frequency. It is also found out that cracks smaller than 20 mm have no dominant effect on the first five natural frequency modes anywhere in the silicon wafer. [DOI: 10.1115/1.4024248]

Keywords: natural frequency, microstructure, silicon wafers, crack size, thickness effect

1 Introduction

Despite the current crisis the crystalline silicon-based photovoltaic solar industry bear the promise of renewable energy resources. At present, single-crystalline (sc-Si) and multicrystalline silicon (mc-Si)-based solar cells make up over 80% of the commercial solar cells in the market [1]. Thinner and larger silicon wafers are preferable for cost reduction [2]. The production cost of silicon wafers consists of 75% of the total cost of solar module. Recent industrial studies have shown that wafer and cell breakage during handling, transport, and other processing steps increased in solar cell production using thinner wafers [3–5]. It is therefore crucial to understand the origin of wafer breakage in order to enhance the production efficiency. Propagation of cracks or damage is the fundamental reason of breakage of Si wafers. Vibration acting as a crack driving force is one of the most common loading modes during handling and subsequent processing steps and has a major impact on wafer breakage rate. Very few studies have been performed on vibration analysis of silicon wafers. The vibration of silicon wafers can draw an analogy to that of thin plates. Leissa [6] presented analytical solutions for the free vibration of thin isotropic rectangular plates. Twenty-one types of boundary conditions combined with simply supported, clamped and free edges were studied. Analytical solutions for the natural frequencies can be obtained only for a few cases. For the free vibration of anisotropic rectangular plates, it is even more difficult to obtain analytical solutions. Numerical methods, such as the Rayleigh–Ritz method, finite element method (FEM), and the differential quadrature method are the chief approaches for solving anisotropic rectangular plate problems [7–17]. Huang and Zhang [18,19] studied the vibration problem of isotropic and orthotropic rectangular plates. They also used the same approach to solve the vibration problem of anisotropic rectangular plates and obtained a general analytical solution [20]. More recently, the free vibration of anisotropic plates with simply supported or clamped boundary conditions was analysed by using the discrete singular convolution (DSC) algorithm [21,22]. So far, only the clamped and simply supported boundary conditions were used for the vibration analysis of anisotropic plates, the free boundary condition has not been employed due to its difficulty in using the DSC algorithm [23]. It must be noted that the solutions for thin plates cannot be directly extended to the case of solar silicon wafers which are made of heterogeneous microstructures, process nonuniform thickness and consist of cracks.

The purpose of this study is to understand the effect of microstructure (grain size and material orientation), thickness variation, and crack geometry on the natural frequency of silicon wafers. The finite element (FE) program ABAQUS has been used for the analyses. The paper is organized as follows: the theoretical aspects of the study including the material properties, models, and available solutions for thin plates are presented first. The model verification, parameter study, results, and discussion are presented in Sec. 3. Some concluding remarks are given at the end of paper.

2 Modelling Procedure and Material Properties

2.1 Wafer Geometry and FE Mesh. The dimensions of the silicon wafers modelled in the present study are $156 \times 156 \times 0.2$ mm^3. In order to consider the effect of material microstructure, 20-node quadratic brick elements (type C3D20R) were utilized. The FEM analysis accounts for the geometric nonlinearity associated with large deformation of thin wafers. Preliminary static analysis showed that the differences in the results obtained from linear and nonlinear simulations are sufficiently large to indicate that a linear simulation is not adequate for these wafers when static analysis is target of study. Similar conclusion in this regard was also drawn in Ref. [24]. However, the ABAQUS uses a linear solution to determine the natural frequencies and this nonlinearity has no dominant effect on the natural frequency calculations. A preliminary mesh convergence study has been carried out, and finally second order brick elements with four elements in thickness direction and 78 elements in length and width directions were selected for the analyses. Two boundary conditions, free

[1]Corresponding author.

Contributed by the Solar Energy Division of ASME for publication in the JOURNAL OF SOLAR ENERGY ENGINEERING. Manuscript received September 13, 2012; final manuscript received April 11, 2013; published online July 2, 2013. Assoc. Editor: Santiago Silvestre.

edge (FFFF) and simply supported edge (SSSS) are used to verify the model.

2.2 Material Property. In this study, both isotropic and anisotropic silicon wafers have been considered. For the anisotropic case, both single and multicrystal structures are studied.

2.2.1 Isotropic Model. A reference case with elastic and isotropic silicon wafers was considered first. The values of Young's modulus, density, and Poisson ratio for cast silicon are taken as, $E = 162.5$ GPa, $\rho = 2330$ kg/m^3, and $\upsilon = 0.223$. These values are widely used in the literature [25].

2.2.2 Anisotropic Model. Multicrystalline silicon wafers are anisotropic in nature. Anisotropic material properties are specified using the stiffness matrix defined in the proper coordinate system (x,y,z) [26]. The stiffness coefficients are obtained from the known compliance coefficients for single crystal silicon with respect to the crystal coordinate system. In general, multicrystalline silicon wafers are characterized by a $\{1\ 1\ 0\}$ surface and a $\langle 1\ 1\ 2\rangle$ growth direction [27]. Therefore, the stiffness is specified using the $\{1\ 1\ 0\}$ single-crystal properties with [1 1 −2], [1 −1 1], and [1 1 0] orientations representing the x, y, and z axes, respectively. The resulting elastic stiffness matrix (in GPa) for the silicon wafer is given

$$C_{ijkl}^{Cz} = \begin{pmatrix} 165.64 & 63.94 & 63.94 & 0 & 0 & 0 \\ & 165.64 & 63.94 & 0 & 0 & 0 \\ & & 165.64 & 0 & 0 & 0 \\ & & & 79.51 & 0 & 0 \\ & & & & 79.51 & 0 \\ \text{sym} & & & & & 79.51 \end{pmatrix} \tag{1}$$

In the analysis of multicrystalline silicon wafers, this stiffness matrix will be rotated for each grain independently. The values of density and Poisson ratio are kept the same as the isotropic case.

2.3 Thin Plate Theory. The available solutions for thin plates are employed to verify the present thin wafer models. This verification was done by comparing the natural frequencies calculated by thin plate theory and the results from FE analyses. For isotropic material, the free harmonic vibration of a thin plate with a constant thickness t is governed by the following differential equation:

$$\bar{D}\nabla^4 W - \omega^2 \rho t W = 0 \tag{2}$$

where $W(x, y)$ is the deflection of the plate, ∇^4 is the biharmonic differential operator; $\bar{D} = (Et^3/12(1-\upsilon^2))$ is the bending rigidity with E and ν being the Young's modulus and the Poisson's ratio, respectively; ω is the circular frequency, and ρ is the mass density.

The governing differential equation for a thin anisotropic rectangular plate with length a, width b, and thickness t, is given by

$$\bar{D}_{11}\frac{\partial^4 W}{\partial x^4} + 4\bar{D}_{16}\frac{\partial^4 W}{\partial x^3 \partial y} + 2(\bar{D}_{12} + 2\bar{D}_{66})\frac{\partial^4 W}{\partial x^2 \partial y^2} + 4\bar{D}_{26}\frac{\partial^4 W}{\partial x \partial y^3} + \bar{D}_{22}\frac{\partial^4 W}{\partial y^4} = \rho t \omega^2 W \tag{3}$$

where $\bar{D}_{12}$, $\bar{D}_{12}$, $\bar{D}_{22}$, $\bar{D}_{16}$, $\bar{D}_{26}$, and $\bar{D}_{66}$ are the stiffness coefficients.

For the convenience of comparisons, the nondimensional frequency, $\bar{\omega}$, is introduced

$$\bar{\omega} = \omega a^2 \sqrt{\frac{\rho t}{\bar{D}}} \tag{4}$$

for thin isotropic rectangular plates. For orthotropic and anisotropic rectangular plates, a similar nondimensional frequency can be used

$$\bar{\omega} = \omega a^2 \sqrt{\frac{\rho t}{\bar{D}_0}}, \quad \left(\bar{D}_0 = \frac{E_{11} t^3}{12(1 - \upsilon_{12}\upsilon_{21})}\right) \tag{5}$$

where υ_{12} and υ_{21} are the Poisson ratios in direction 1 and 2, respectively. For thin isotropic rectangular plates, an exact solution for the nondimensional frequency is available [10]

$$\bar{\omega}_{\text{exact}} = \pi^2 \left[m^2 + n^2 \left(\frac{a}{b}\right)^2\right] \quad (m, n = 1, 2, \ldots) \tag{6}$$

The exact nondimensional frequency for thin orthotropic rectangular plates is given [28]

$$\bar{\omega}_{\text{exact}} = \pi^2 \sqrt{\frac{\bar{D}_{11}}{\bar{D}_0} m^4 + 2\left(\frac{\bar{D}_{12}}{\bar{D}_0} + 2\frac{\bar{D}_{66}}{\bar{D}_0}\right)\left(\frac{a}{b}\right)^2 m^2 n^2 + \frac{\bar{D}_{22}}{\bar{D}_0}\left(\frac{a}{b}\right)^2 n^4} \quad (m, n = 1, 2, \ldots) \tag{7}$$

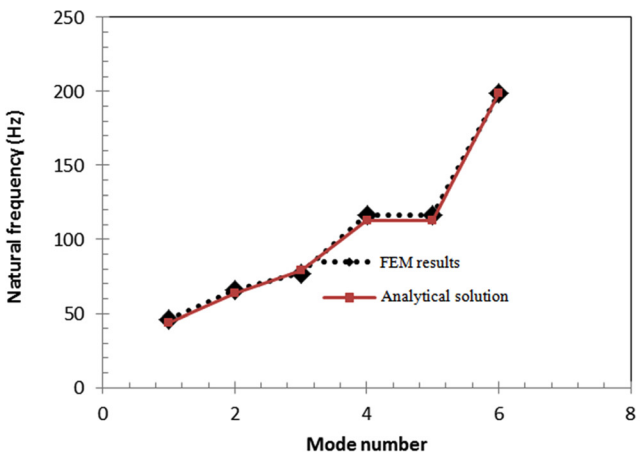

(a)

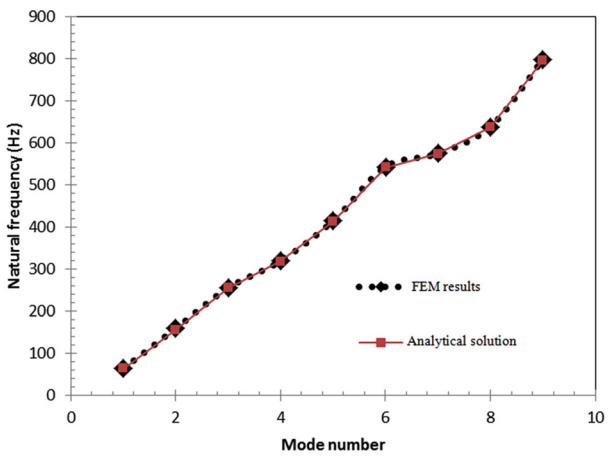

(b)

Fig. 1 Comparison of the natural frequency calculated by analytical solution and FEM for isotropic model with (*a*) FFFF boundary conditions and (*b*) SSSS boundary

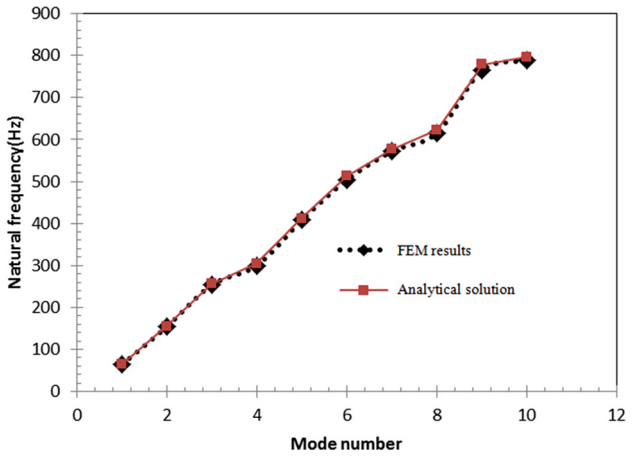

Fig. 2 Comparison of the natural frequency between analytical solution and FEM for anisotropic model with SSSS boundary conditions

Equations (4) and (7) are used as the reference solutions for the present isotropic and anisotropic silicon wafers, respectively. A percentage relative error (Re) is defined to compare the results between the analytical and FE solutions

$$\mathrm{Re}(\%) = \frac{\bar{\omega}_{\mathrm{FEM}} - \bar{\omega}_{\mathrm{exact}}}{\bar{\omega}_{\mathrm{exact}}} \times 100\% \tag{8}$$

where $\bar{\omega}_{\mathrm{FEM}}$ and $\bar{\omega}_{\mathrm{exact}}$ are the nondimensional natural frequencies calculated by FEM and the reference solutions, respectively. The acceptable relative error is set to be 2.5% in this investigation.

3 Results and Discussion

3.1 Model Verification. To verify the model, two boundary conditions, FFFF and fully SSSS have been used for isotropic single crystal wafers and only SSSS boundary condition is considered for anisotropic single crystal wafers. Many attempts have been made to optimize the mesh and element type to achieve the acceptable relative accuracy set to be 2.5% in this study. Normalized frequency is used to present results. The normalized frequency is defined as the ratio of natural frequency of anisotropic case divided by that of the isotropic one. The comparison between the natural frequencies calculated by the FEM and exact solution for the isotropic wafer are presented in Fig. 1(*a*) for FFFF boundary conditions and Fig. 1(*b*) for SSSS boundary condition. Figure 2 compares the natural frequencies for the anisotropic case with SSSS boundary conditions. All the results from Figs. 1 and 2 show a good agreement between the exact solutions and the FEM results. We may conclude that the model, we used is sufficient for the purpose of the present investigation. It should be noted that only the first five natural frequencies are focused in the present study. Although these five natural frequencies are all out of plane, they are not the same in regarding to stress state and distribution in wafers. For instance, as it observed in Fig. 3, the first mode is like a semi twisting loading and therefore shear stress is the dominant stress. But the second and third mode are biaxial bending and

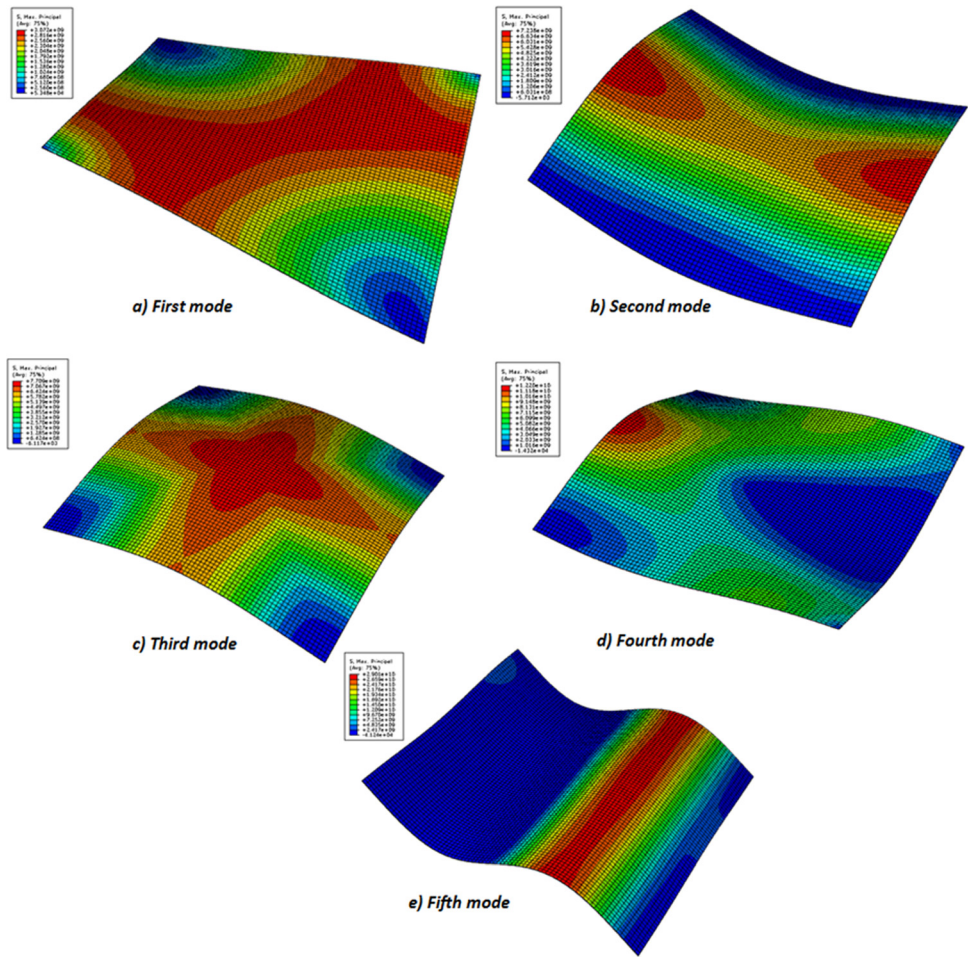

Fig. 3 maximum principle stress for first five shape modes of isotropic silicon wafers with FFFF boundary condition

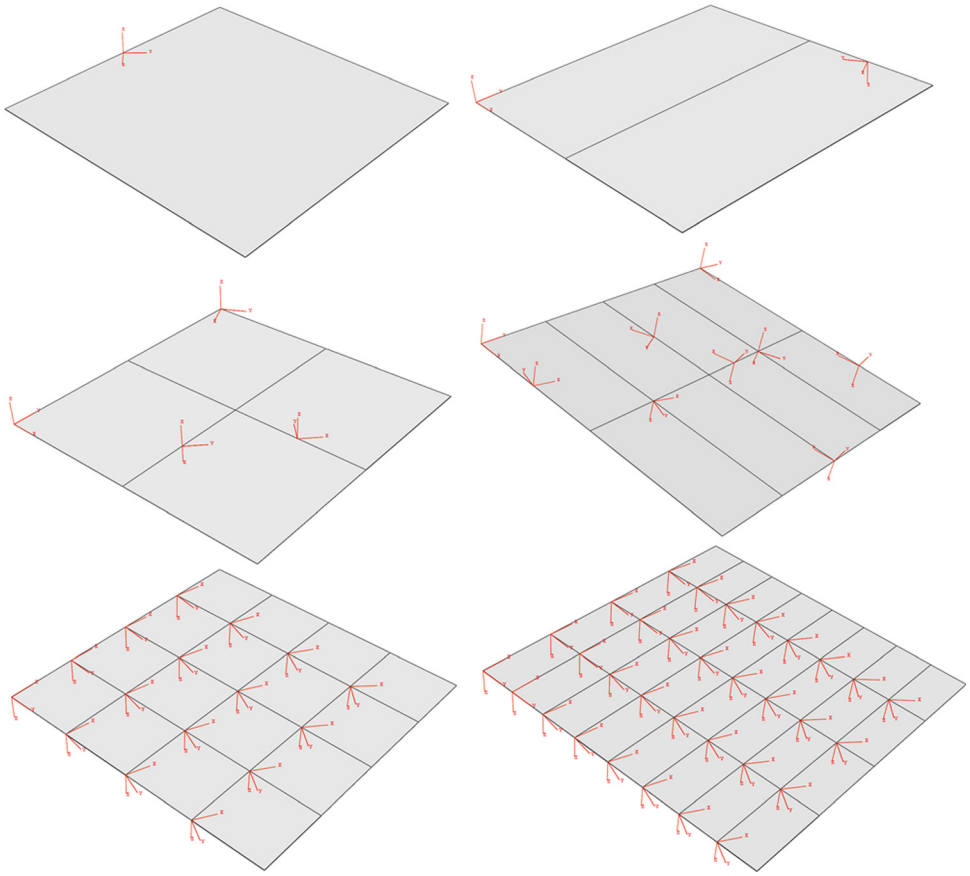

Fig. 4 Example of grain size and material orientations for the models with 1, 2, 4, 8, 16, and 32 grains

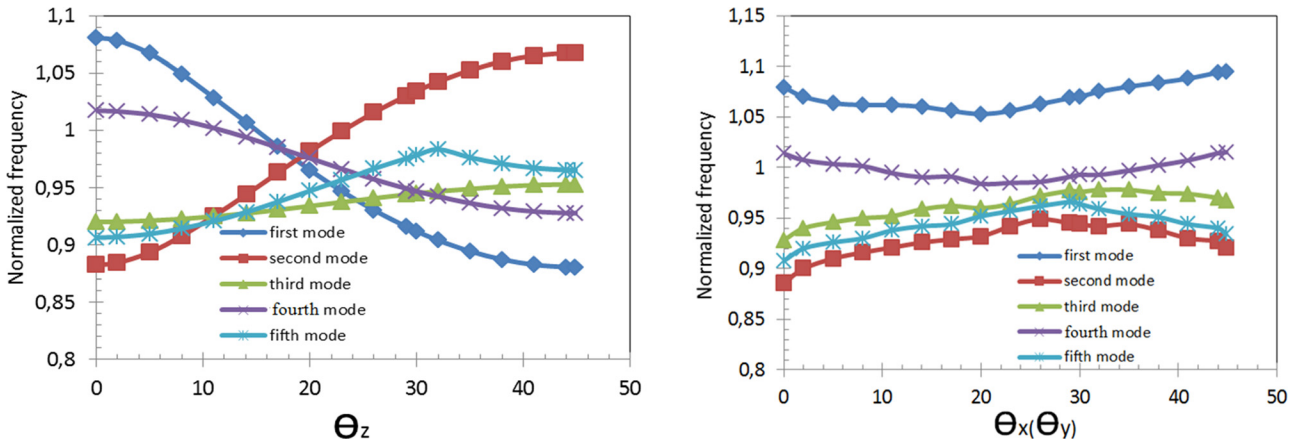

Fig. 5 Effect of material orientation on the normalized frequency for single crystal silicon rotating (*a*) along *z* axis and (*b*) along *x*/*y* axis

semi pure bending, respectively. In addition to, fourth and fifth modes are a mixture of bending and twisting.

3.2 Effect of Microstructure on Natural Frequency: Results and Discussion. In order to investigate the effect of microstructure on the natural frequency of silicon wafers, six cases (single crystalline silicon, 2, 4, 8, 16, and 32 grains) are considered and different material orientations are studied in each case. Figure 4 shows an example of material orientations in each case.

3.2.1 Single Crystal Silicon. In the single crystal silicon case (only 1 grain), the grain orientation is rotated along the z and x/y axis from 0 deg to 45 deg by an increment 2 deg. There are 44 (22×2) rotations (22 rotation on each axis) in total. The first five natural frequencies are calculated for each rotation. The first five modes should be sufficient for vibration analysis of wafer handling process. The results are illustrated in Figs. 5(*a*) and 5(*b*), respectively. Figure 5(*a*) shows the effect of material orientation rotated along the z axis. The zero rotation state represents the coordinate system defined in Sec. 2.2.2. It is interesting to note that the first mode natural frequency for the single crystal wafer at the zero rotation state is about 8% higher than the one of corresponding isotropic wafer. This value decreases with the increase of the rotation, and approaches the same value of isotropic wafer

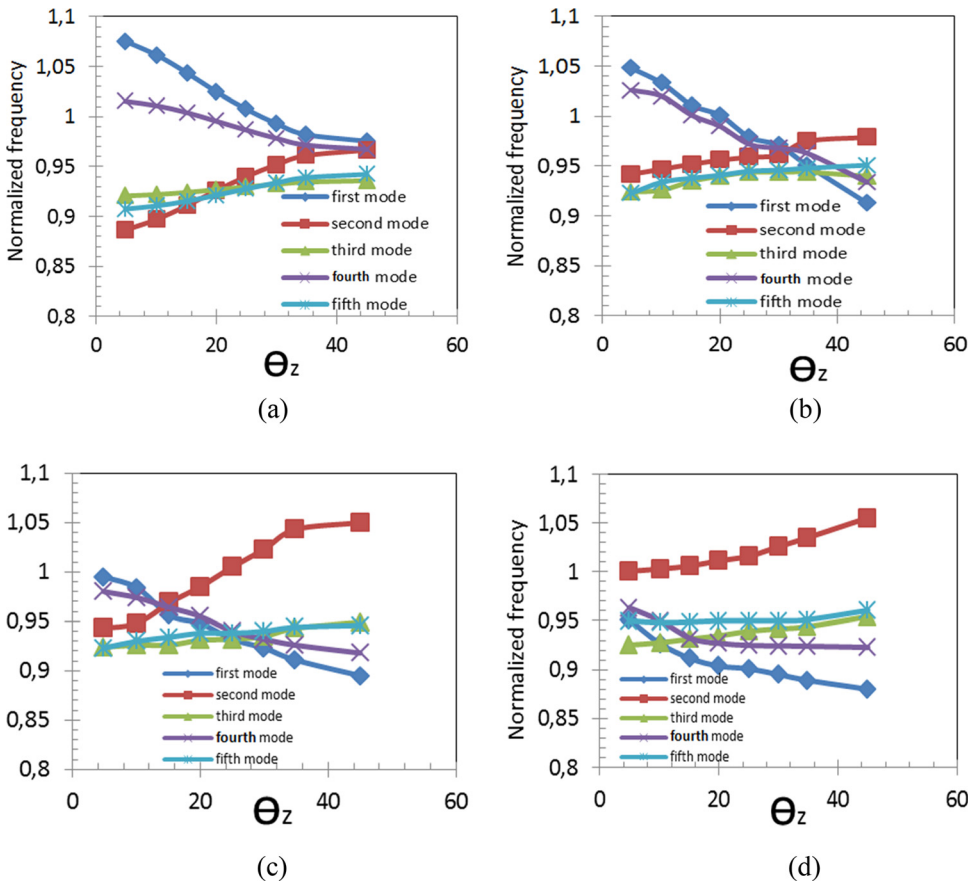

Fig. 6 Effect of material orientation rotating along *z* axis on the normalized frequency for the wafer with 2 grains (grain 1 fixed at *a* = 0 deg, *b* = 15 deg, *c* = 30 deg, and *d* = 45 deg)

at $\theta_z = 14$ deg. It further decreases to a minimum which is about 11% smaller than that of the isotropic wafer at 45 deg. The trend of the second mode natural frequency is similar to the first model, but in an opposite way. The effect of grain orientation on the natural frequency of other modes is less significant compared with the first two modes. The curves for all the five modes cross approximately at $\theta_z = 19$ deg, and all the five normalized natural frequencies approach a similar value below 1.0, which indicates that at this specific grain orientation the natural frequency calculated using isotropic assumption will overestimate the natural frequency of anisotropic silicon in every mode. Figure 5(*b*) displays the effect of material orientation rotated along the *x*/*y* axis on the natural frequency. Unlike the results shown in Fig. 5(*a*) where each curve shows a monotonic increasing or decreasing trend and all the curves cross at a specific grain orientation, the curves in Fig. 5(*b*) are almost parallel to each other. The normalized first mode natural frequency is always higher than 1. It implies the first mode natural frequency for anisotropic wafer will be always larger than the one for corresponding anisotropic wafer. The other mode natural frequencies reach a minimum or maximum value at $\theta_{x/y} = 20$–25 deg. The minimum and maximum values are close to 1, which indicates that the natural frequency values are almost the same for the isotropic and anisotropic cases at this material orientation. In general, Fig. 5(*b*) shows that material orientation along *x*/*y* axis does not play a strong role on the natural frequency of anisotropic wafer. The small difference is caused by the dimension of wafers (thickness is much smaller than two other dimensions), and therefore, anisotropy can be neglected in the thickness direction.

3.2.2 Two-Grain Silicon Wafer. For the cases with two and four grains, the same approach as for single crystal grain is employed to study the effect of material orientation. For the case with 2 grains, two equal rectangular grains (Fig. 4) are considered and the material orientation increment is set to be 5 deg instead of 2 deg. We fix the coordinates of one grain (which is called first grain) at 0 deg direction and rotate the other (the second grain) by 5 deg along z axis from 0 deg to 45 deg (nine positions in between). Afterward, the first grain which was fixed at 0 deg will be rotated by 5 deg and hold in this new position, and the second grain is rotated by 5 deg until reaching 45 deg. This algorithm is repeated until the first grain reaches 45 deg. For each set of material orientation, the same procedure is employed to calculate the natural frequency. Figures 6 and 7 show the effect of material orientation on the natural frequency for 2 grains rotating along *z* and *x*/*y* axis, respectively. Similar to the single crystal case (Fig. 5(*a*)), the modes 1 and 4 natural frequencies monotonically decrease with the rotation along the *z* axis, frequencies for other three modes increase with the rotation. For the single crystal case shown in Fig. 5(*a*), all the curves cross at the *z* rotation between 20 deg and 25 deg (symmetrical line). It is interesting to observe that for the two-grain anisotropic wafer all the five modes tend to converge to an average value 0.95 at *z* rotation approximately 45 deg, 37.5 deg, 12.5 deg, and 0 deg for the four cases shown in Fig. 6, respectively. These configurations are compounded of the 2 single grains with different grain orientation. Figure 6 also shows that the two-grain anisotropic wafer displays less variation in natural frequency with respect to the *z* angle than the single crystal. For instance, the variations for first mode are 8.4% in Fig. 6(*a*), 12.5% in Fig. 6(*b*), 10.6% in Fig. 6(*c*), and 7.3% in Fig. 6(*d*), respectively. However, the variation for the single crystal wafer is 18.4%. Figure 7 shows the effect of material orientation along *x*/*y* axis. A similar trend to that shown in Fig. 5(*b*) for the single crystal wafer can be seen for the two-grain wafer. The effect of the

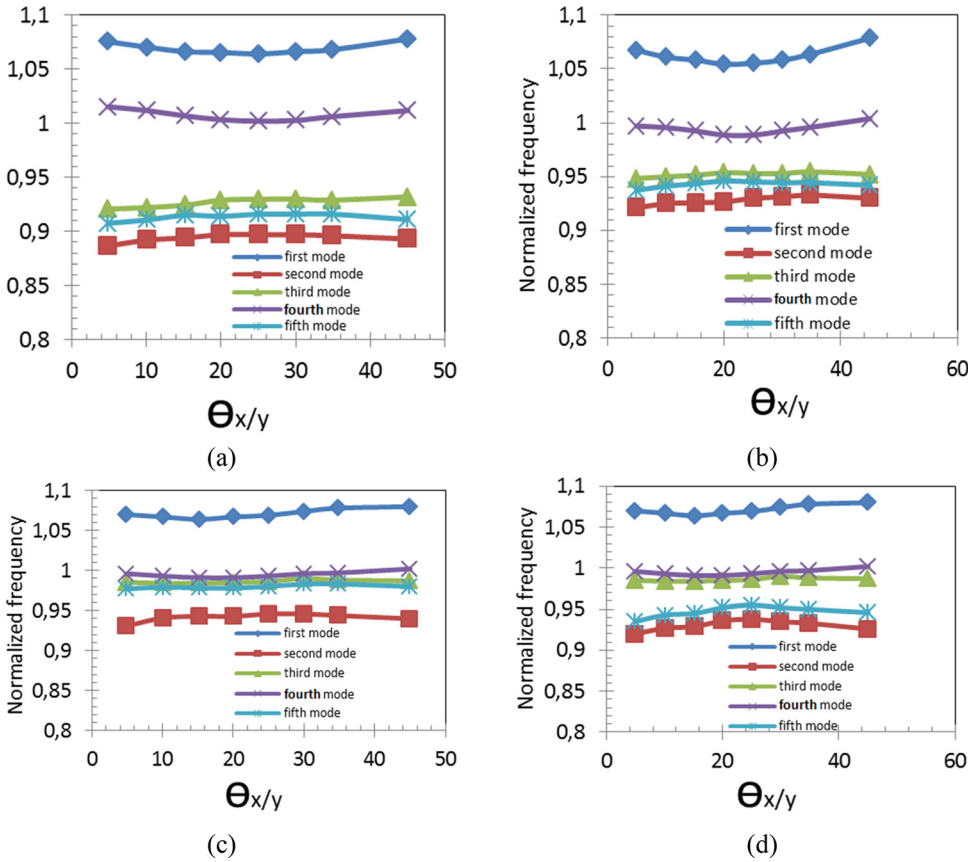

Fig. 7 Effect of material orientation rotating along *x*/*y* axis on the normalized frequency for the wafer with 2 grains (grain 1 fixed at *a* = 0 deg, *b* = 15 deg, *c* = 30 deg, and *d* = 45 deg)

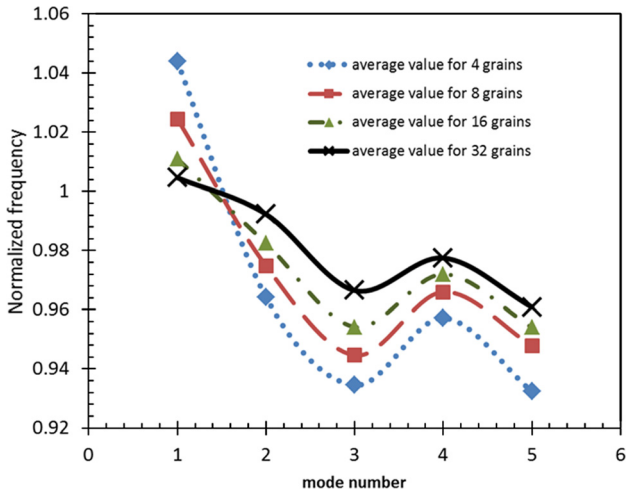

Fig. 8 Effect of material orientation for 4, 8, 16, and 32 grains on the first five natural frequencies

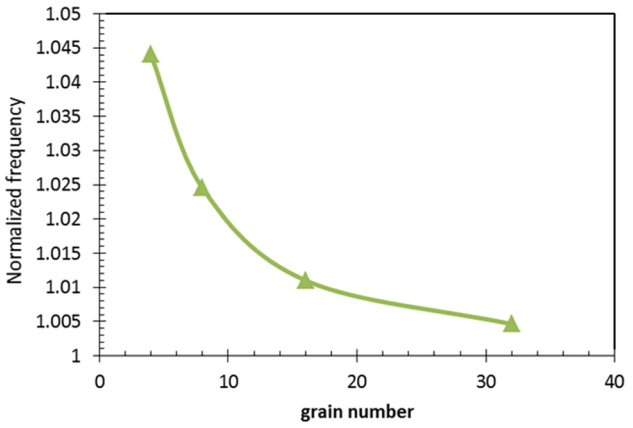

Fig. 9 Effect of material orientation rotate on *z* axis for 4, 8, 16, and 32 grains on the first mode

material orientation along *x*/*y* axis is marginal and all the curves are parallel to each other. The normalized natural frequency for mode 1 is always the largest, larger than 1. The second mode normalized natural frequency became the smallest and always below 1 with other modes lying in between the first and second modes. It is interesting to note that the fourth mode normalized natural frequency is very close to 1, independent of the material orientation. This observation indicates that the fourth mode natural frequency for the anisotropic two-grain wafer can be calculated from the corresponding isotropic wafer.

3.2.3 Multigrains. In this section general cases with multi grains up to 32 grains have been considered using a random method. For each grain, 20 nonoverlapping random crystalline orientations are generated by a MATLAB code. The results can be seen in Figs. 8 and 9. In these figures, the average value of each mode corresponding to 20 random orientations are compared for the cases with 4, 8, 16, and 32 grains. Figure 8 shows the effect of materials orientation along *z* axis on the normalized natural frequency. It can be seen that for all cases with multi grains up to 32 the mode 1 normalized natural frequency of multigrain silicon wafers is always larger than 1, and normalized modes 2–4 natural frequencies are always smaller than 1. However, with the increase of the number of grains, the natural frequency of anisotropic multi

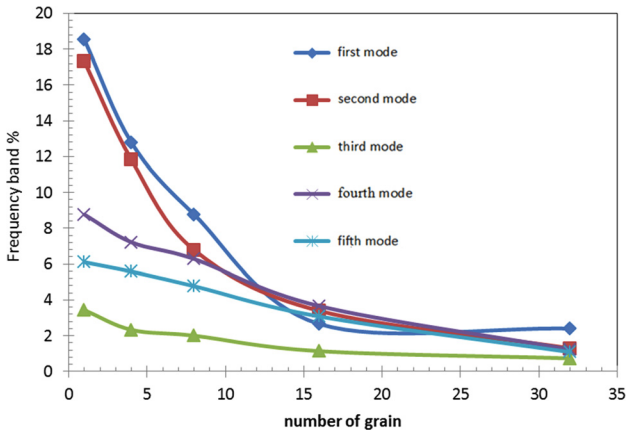

Fig. 10 Frequency band for the first five natural frequencies

grain silicon wafers for both mode 1 and modes 2–5 are approaching the values of the corresponding isotropic silicon wafers. This phenomenon can also be understood from Fig. 9 which displays the normalized natural frequency of mode 1 as a function grain number. The normalized frequency monotonically approaches to 1 with the increase of grain number. It can be generally concluded that the natural frequency calculated assuming isotropic elastic properties of silicon is a good representation of the natural frequency of anisotropic multi crystalline silicon wafers with an error less than 3.8% (the maximum error correspond to 32 grains). In a real solar silicon wafer, the grain numbers are much higher than 32; therefore, the error should be less than 3.8%. Frequency band is another useful parameter to understand the effect of multi grains on natural frequency. A difference between the maximum and minimum natural frequencies related to different material orientation is defined as a frequency band. Figure 10 plots the frequency band as a function of the grain number. The results for the single crystal wafer and wafers with two and four grains are also included. For the single crystal wafer, a frequency band of 0.187 can be expected for the first mode. A dramatic reduction of the frequency band for modes 1 and 2 can be seen with a more or less linear reduction for other three modes. When the number of grain is 32, the frequency band of all the modes approaches to 0.02 (2% of the corresponding the isotropic case).

3.3 Thickness Variation Effect. Due to the nature of sawing process, the cross section of silicon wafers (thickness direction) is nonuniform (a trapezoid). Thickness variation can influence the natural frequency. Wafer stiffness will be enhanced by increasing the thickness, which can further increase the natural frequency.

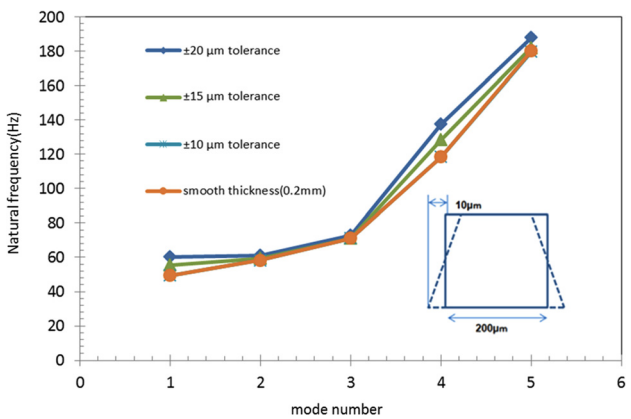

Fig. 11 The effect of thickness variation on the natural frequency of an isotropic model

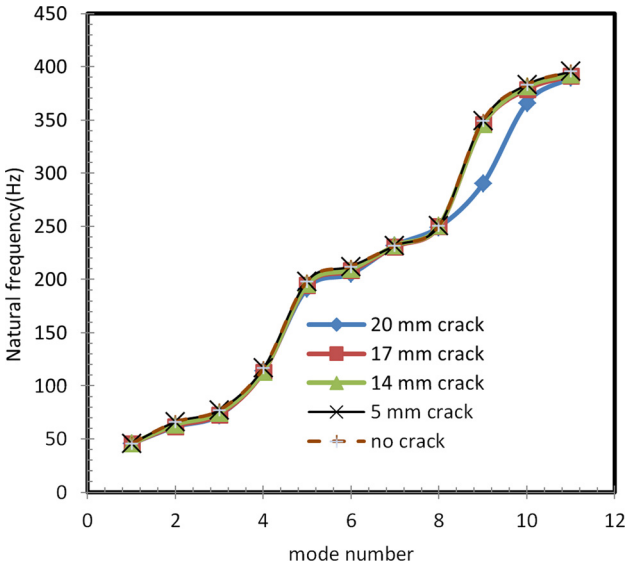

Fig. 12 The effect of crack size on the natural frequency of an isotropic wafer model with a crack in the center

On the other hand, increase of mass by increasing thickness will lead to reduction of natural frequency. The inlet in Fig. 11 shows the definition of the thickness variation for single crystal wafer. Thickness variation up to 20 μm has been analysed. Figure 11 shows variation of the first five natural frequencies as a function of the thickness variation. As it can be seen, at ± 10 μm, the variation of thickness has no remarkable effect on natural frequencies. For modes 2 and 3, the natural frequency is not influenced by the thickness variation considered, since most deflection in this mode is related to the middle layer of the silicon wafer which is dominated by the nominal value (nominal value corresponds to the smooth and uniform thickness, 0.2 mm). A relatively larger difference in natural frequency value is observed for the fourth mode.

3.4 Effect of Crack Geometry. Silicon wafers can possess cracks and it is interesting to understand how the natural frequency is influenced by the presence of initial cracks. Understanding the influence of cracks may facilitate the crack detection. Previous results showed that normalized frequency approaches to 1 with the increase of grain number. Therefore, multicrystal silicon wafer is represented by an isotropic silicon wafer model.

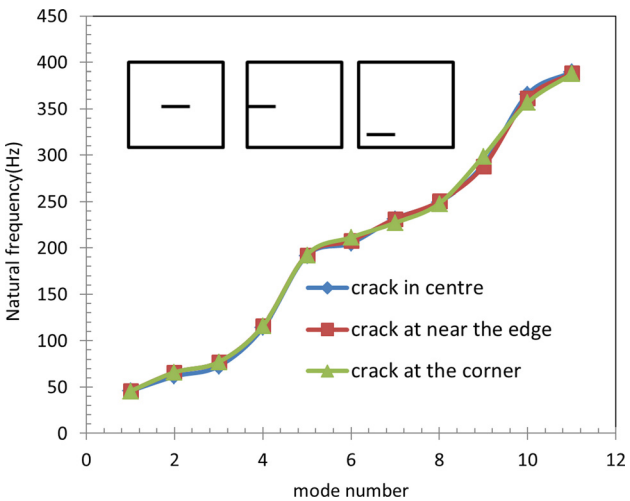

Fig. 13 The effect of crack position on the natural frequency with crack size = 20 mm

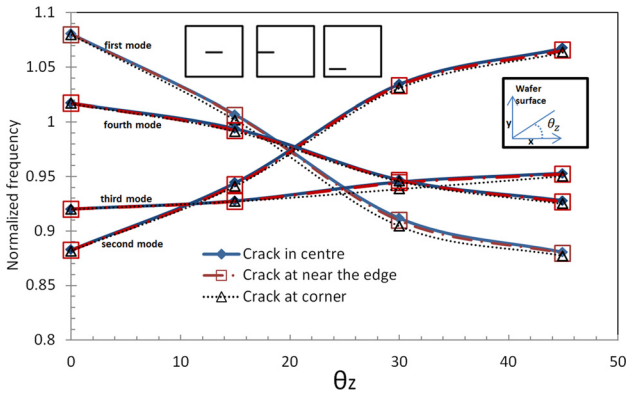

Fig. 14 The effect of crack position on the normalized frequency with crack size = 20 mm and different material orientation

To understand the effect of crack size on natural frequency, it is assumed that all cracks are located at the center of the silicon wafer and only the crack size has changed. The effect of the size of a center crack on the natural frequency is plotted in Fig. 12. The result of the wafer without a crack is also included for comparison. It shows that the natural frequency up to the 8th mode is not significantly influenced by a central crack less than 20 mm. In addition, three crack locations (center, next to edge and corner of the wafer) are considered to investigate the effect of crack location on natural frequency. Figure 13 depicts the effect of position of a 20 mm crack size on the natural frequency. As it can be observed from Fig. 13, the natural frequency is not sensitive to the crack position for crack less 20 mm. Finally, Fig. 14 presents the effect of crack position (20 mm length) on the normalized frequency for the single crystal silicon wafer with different material orientations. It also shows that material orientation is not sensitive to the crack position.

4 Conclusions

Vibration is one of the most common loading modes during handling of solar silicon wafer and has a significant influence on breakage rate during subsequent handling and processing steps. In this study, we address an important question as whether an anisotropic multi crystalline silicon wafer can be treated as an isotropic wafer in a vibration analysis by focusing on the correlation between the natural frequency and solar silicon wafer microstructure (grain size and grain orientation), thickness variation, and crack geometry (position and size). Following conclusions can be drawn:

- The natural frequency of single crystal silicon wafer is strongly dependent on the material orientation. The dependence on the material orientations is reduced in the case of multi crystalline silicon wafer. When the number of grains is larger than eight, the maximum error of the natural frequency of an anisotropic wafer modelled by an isotropic wafer in a vibration analysis is below 5%.
- Single crystal silicon wafer has the highest frequency band and the frequency band reduces with the increase of the grain number.
- Up to 10% thickness variation has no observable effect on the natural frequency. Thickness tolerance less than 10% can be neglected in a vibration analysis and the wafer can be treated as a uniform plate.
- Natural frequency is not strongly influenced by the crack position for crack less than 20 mm. A significant effect can occur at higher modes.

Acknowledgment

The authors would like thank the NEXTGEN_SI project financed by the REC group and Norwegian Research Council.

References

[1] Moller, H. J., Funke, M., Rinio, C., and Scholz, S., 2005, "Multi-Crystalline Silicon for Solar Cells," Thin Solid Films, **487**, pp. 179–187.
[2] Dhere, N. G., and Toward, G. W., 2007, "Production of CIGS Within the Next Decade," Sol. Energy Mater. Sol. Cells, **91**, pp. 1376–1382.
[3] Dominguez, P. S., and Fernandez, J. M., 2005, "Introduction of Thinner Mono-Crystalline Silicon Wafers in an Industrial Cell-Manufacturing Facility," Proceedings 20th European Photo Voltaic Solar Energy Conference, Barcelona, Spain, June 6–10.
[4] Wang, P. W., 2006, "Industrial Challenges for Thin Wafer Manufacturing," Proceedings 4th World Conference on Photovoltaic Energy Conversion, Waikoloa, HI, May 7–12, pp.1179–1182.
[5] Sopori, B., Sheldon, P., and Rupnowski, P., 2006, "Wafer Breakage Mechanism(s) and a Method for Screening Problem Wafers,'' Proceedings 16th Workshop on Crystalline Silicon Solar Cells and Modules, Denver, CO, August 6–9, pp. 129–138.
[6] Leissa, A. W., 1973, "The Free Vibration of Rectangular Plates," J. Sound Vib., **31**, pp. 257–293.
[7] Palardy, R. F., and Palazotto, A. N., 1990, "Buckling and Vibration of Composite Plates Using the Levy Method," Compos. Struct., **14**, pp. 61–68.
[8] Chow, S. T., Liew, K. M., and Lam, K. Y., 1992, "Transverse Vibration of Symmetrically Laminated Rectangular Composite Plates," Compos. Struct., **20**, pp. 213–226.
[9] Bert, C. W., Wang, X. W., and Striz, A. G., 1993, "Differential Quadrature for Static and Free Vibration Analysis of Anisotropic Plates," Int. J. Solids Struct., **30**, pp. 1737–1744.
[10] Akhras, G., Cheung, M. S., and Li, W., 1993, "Static and Vibration Analysis of Anisotropic Composites by Finite Strip Method," Int. J. Solids Struct., **30**, pp. 3129–3137.
[11] Farsa, J., Kukreti, A. R., and Bert, C. W., 1993, "Fundamental Frequency Analysis of Laminated Rectangular Plates by Differential Quardrature Method," Int. J. Numer. Methods Eng., **36**, pp. 2341–2356.
[12] Shupikov, A. N., and Ugrimov, S. V., 1999, "Vibrations of Multiplayer Plates Under the Effect of Impulse Loads, Three Dimensional Theory," Int. J. Solids Struct., **36**, pp. 3391–3402.
[13] Wen, P. H., Aliabadi, M. H., and Young, A., 2000, "A Boundary Element Method for Dynamic Plate Bending Problems," Int. J. Solids Struct., **37**, pp. 5177–5188.
[14] Chattopadhyay, A., and Radu, A. G., 2000, "Dynamic Instability of Composite Laminates Using a Higher Order Theory," Comput. Struct., **77**, pp. 453–460.
[15] Cheung, Y. K., and Zhou, D., 2001, "Vibration Analysis of Symmetrically Laminated Rectangular Plates With Wafers," Comput. Struct., **79**, pp. 33–41.
[16] Civalek, Ö., 2004, "Application of Differential Quadrature (DQ) and Harmonic Differential Quadrature (HDQ) for Buckling Analysis of Thin Isotropic Plates and Elastic Columns," Eng. Struct., **26**(2), pp. 171–186.
[17] Yeh, Y. L., Jang M. J., and Wang, C. C., 2006, "Analysing the Free Vibrations of a Plate Using Finite Difference and Differential Transformation Method," Appl. Math. Comput., **178**, pp. 493–501.
[18] Huang, Y., 1988, "A General Analytical Solution for Elastic Vibration of Rectangular Thin Plates," Appl. Math. Mech. (English edition), **9**, pp. 1057–1065.
[19] Huang, Y., and Zhang, X. J., 2002, "General Analytical Solution of Transverse Vibration for Orthotropic Rectangular Thin Plates," J. Mar. Sci. Appl., **1**, pp. 78–82.
[20] Huang, Y., Lei, Y., and Shen, H., 2006, "Free Vibration of Anisotropic Rectangular Plates by General Analytical Method," Appl. Math. Mech. (English edition), **27**(4), pp. 461–467.
[21] Gürses, M., Civalek Ö., Korkmaz, A. K., and Ersoy, H., 2009, "Free Vibration Analysis of Symmetric Laminated Skew Plates by Discrete Singular Convolution Technique Based on First-Order Shear Deformation Theory," Int. J. Numer. Methods Eng., **79**, pp. 290–313.
[22] Seçgin, A., and Sarıgül, A. S., 2008, "Free Vibration Analysis of Symmetrically Laminated Thin Composite Plates by Using Discrete Singular Convolution (DSC) Approach: Algorithm and Verification," J. Sound Vib., **315**, pp. 197–211.
[23] Qin, Z., and Xinwei, W., 2011, "Free Vibration Analysis of Thin Isotropic and Anisotropic Rectangular Plates by the Discrete Singular Convolution Algorithm," Int. J. Numer. Methods Eng., **86**, pp. 782–800.
[24] Chao, C. C., Chleboski, R., Henderson, E. J., Holmes, C. K., and Kalejs, J. P., 1991, "Fracture Behaviour of Silicon Cut With High Power Laser," Proc. Material Research Society Symposium, MRS, Pittsburgh, **226**, pp. 363–368.
[25] Claudia, F., Eckehard, K., Meinhard, K., and Joachim, M. H., 2004, "Biaxial Fracture Test of Silicon Wafers," Adv. Eng. Mater., **6**(7), pp. 594–598.
[26] Wortman, J. J., and Evans, R. A., 1965, "Young's Modulus, Shear Modulus, and Poisson's Ratio in Silicon and Germanium," J. Appl. Phys., **36**, pp. 153–156.
[27] Ravi, K. V., 1977, "The Growth of EFG Silicon Ribbons," J. Cryst. Growth, **39**, pp. 1–16.
[28] Leissa, A. W., and Narita, Y., 1989, "Vibration Studies for Simply Supported Symmetrically Laminated Rectangular Plates," Compos. Struct., **12**, pp. 113–132.